Impact of photomask quadrature edge effects through focus

Marshal Miller
Andrew R. Neureuther
Daniel Ceperley
Koji Kikuchi

Electrical Engineering and Computer Sciences
University of California at Berkeley

Impact of photomask quadrature edge effects through focus

<u>Marshal A. Miller</u>[1], Andrew R. Neureuther, Daniel P. Ceperley, Koji Kikuchi
UC Berkeley, 271 Cory Hall, Berkeley CA 94704

ABSTRACT

The loss of through focus process latitude due to the interaction of electromagnetic fields that are at 90 degree phase with the intended 0° and 180° at mask edges and line-ends is characterized for 45 nm imaging using thick-mask and image simulation. TEMPEST and Panoramic Technologies simulators are used to determine near fields and images of chromeless, MoSi and Ta-SiO$_2$ line ends. These fields are then analyzed in both space and plane wave spectra to determine rules of thumb for the effective narrowing (real) and leakage (quadrature) contributions in boundary layers to improve the accuracy of thin-mask models. Typical values for ATT-PSM are 0.05 to 0.1 λ/NA per edge. These values varied only slowly out to angles of incidence on the mask of 20° suggesting an angle independent boundary layer parameter would be moderately accurate. For chromeless the values are larger and can be over 0.2 λ/NA per edge for the quadrature component. The through focus imaging for lines and line ends is then made using the full set of near fields, producing a tile of the Bossung curve through focus that is 18 nm for line-end shortening. The Ta-SiO$_2$ mask stack showed more irregular behavior compared to the other masks.

Keywords: Phase-shifting mask, edge effects, thin-mask model, FDTD, electromagnetic simulation, focus shift

1. INTRODUCTION

With mask dimensions shrinking as the industry moves to the 45nm node and beyond, electromagnetic effects which were previously small contributions play a more significant role in on wafer imaging. The addition of complex mask materials for various phase shift masks (PSMs) combined with larger angles of incidence further complicates the modeling of photomask field transmission. When features are large relative to wavelength, a smaller percentage of the light is impacted by edge interaction. Assuming the edge impact is independent of opening size, as immersion lithography pushes the limits of imaging with 193nm the edge contribution will have a larger overall effect on the image. A 10% wavelength effect on each of the two edges is on the order of 1/10 of the mask opening size for 90 nm technology but becomes 1/5 of the mask opening for 45 nm technology.

It has been reported that in manufacturing an Alternating phase shift mask (Alt-PSM), the feature size and pitch must be specified in advance in order to tune the phase shift to account for out of phase, or quadrature, field components produced by the edges.[1] This implies that for features other than those specified, the phase shift is not exact which can lead to asymmetry in the image.[2,3] To achieve the ideal transmission of an 180° phase-shifting shift photomask the extinction
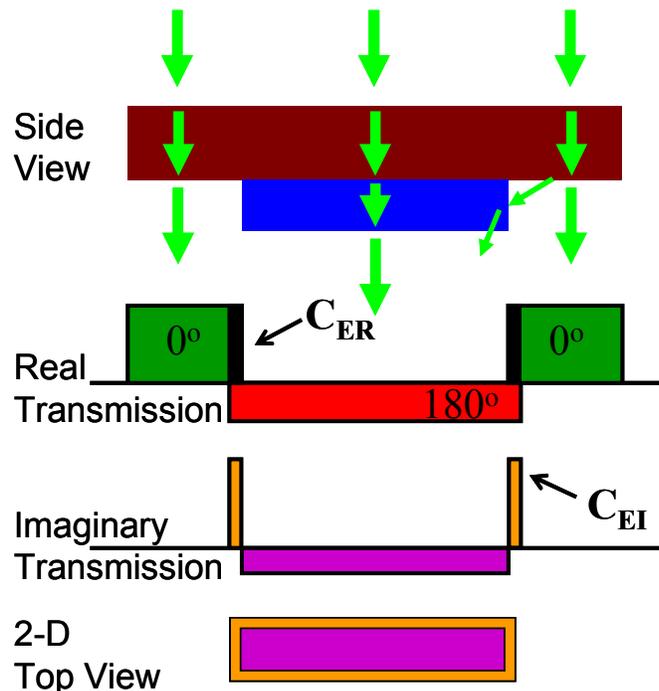
Figure 1: TMA expect 0° (green) and 180° (red), but in practice real and imaginary biases (C$_{ER}$ and C$_{EI}$) are introduced by edge interaction, and must be corrected by shifting edges and adjusting phase shift (purple).

---

[1] mamillr@eecs.berkeley.edu

condition for the 0th order field component must be met by adjusting both bias and phase. It is well know that Alt-PSMs have edge effects on the order of 10% of a wavelength per edges from the simulation work of A. Wong that first revealed the intensity imbalance effect.[4] Even the slight transmission of the chrome can contribute to the performance of a PSM.[5] Thick mask edge contributions and edge-to-edge cross talk have been have been examined by a number of authors[6-8] including various methods of defining equivalent thin mask models. These correction terms can be used to aid mask design by providing more information about electromagnetic effects than a simple thin mask approximation (TMA). In practice these undesired effects can be counteracted by adjusting the phase shift regions or using absorbing materials, such as chrome to cover the edges and reduce electromagnetic impact. An approach for using a sidewall chrome coating has been proposed as a method for reducing the impact of edges[9,10], but at a cost of increasing mask complexity from additional processing steps.

A method for quantifying the edge contributions to fit a boundary layer model was previously presented based on observing the 0th order field transmission through mask openings.[11] This paper presents an expansion of this method to off-axis illumination, alternate mask stacks, and 3-D mask geometries. Section 2 presents a brief description of the method and procedure for extracting real and imaginary field contributions due to edges. Section 3 analyzes simulation data for a chromeless Alt-PSM and a MoSi Att-PSM. Section 4 takes the analysis a step further to include 3-D effects and a look at line end shortening (LES). Section 5 explores at the Ta-SiO$_2$ mask which was problematic for this method due to more complex edge effects.

2. METHOD

In order to satisfy electromagnetic boundary conditions for Maxwell's equations, the wavefront bends at the interface between phase regions to create a continuous phase front. This changes the path difference through the phase-shifting regions, which induces an imaginary, or quadrature, field component in the transmitted fields. In addition energy moves between the regions creating a transmission imbalance compared to TMA. The real and imaginary fields produced at the edges can be modeled as additional transmission sources placed on the border of mask features in a thin mask model. In this paper, the boundary layers described represent edge sources with 0° or 90° phase and amplitude normalized to 1, with the width changed to reflect the strength of these sources.

The sources can be measured with simulation by looking at the 0th order transmission through pitch. Thin mask theory predicts zero transmission where the amplitude of the 0° and 180° fields have equal and opposite values; however, thick mask structures exhibit a minimum at a different point, as seen in Figure 2 for chromeless phase shift lithography (CPL).
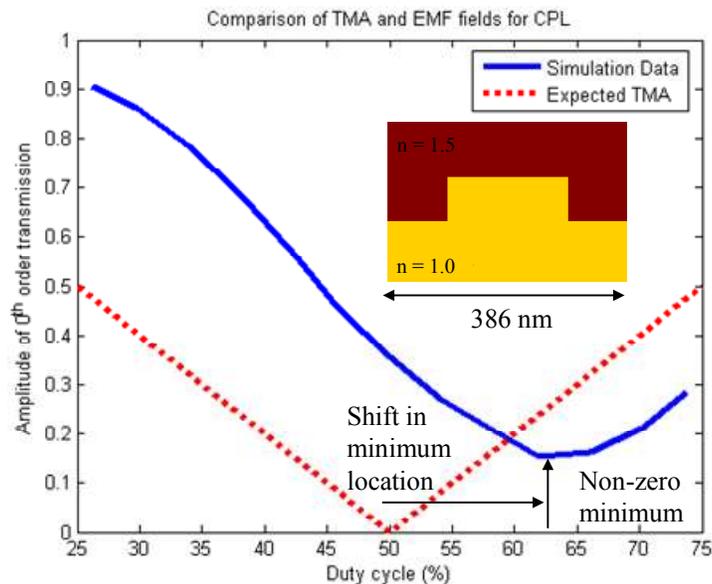
Figure 2: Comparison of 0th order field transmission through duty cycle. TMA transmission vs. thick mask TEMPEST simulation for CPL.

Since the material is lossless, at 50% duty cycle, the positive and negative field components should fully cancel, illustrated by the red dotted line. In the same plot, the solid blue curve shows simulation data for 8° off-axis incidence for a pitch of 386 nm. Thick mask simulations show a shift in both the location and value of this expected null. By observing the minimum value of the 0th order field, the leakage (C_{EI}) due to the imaginary edge contribution can be computed. From the location of this minimum value compared to the TMA prediction, it is possible to calculate the effective narrowing (C_{ER}). In a previous paper[12], we showed that the shift in minimum location can be modeled as a real bias assigned to each mask edge. The relation between the shift and the bias is given by equation (1). Furthermore, the transmission at the minimum is not exactly zero due to out-of-phase light leakage which is not fully canceled by moving the edges. We model this as a quadrature bias applied to each edge. The depth of the null determines the width of the quadrature bias, calculated in equation (2).

$$C_{ER} = (duty_{TMA} - duty_{EMF})*Pitch/ 2 \qquad (1)$$

$$C_{EI} = E_{min}*Pitch/2 \qquad (2)$$

To carry out the analysis of mask vector effects, FDTD simulation with TEMPEST, a rigorous FDTD simulator developed at UC Berkeley, was used for two types of simulations. The first is a 2-D simulation of a mask opening with periodic boundary conditions producing a 1-D grating pattern, which allowed for fast simulations. Duty cycle was varied to locate the extinction condition in the 0th order transmission. The effects of pitch and incidence angle were investigated. In addition, 3-D simulations of isolated line patterns were tested and examined using a similar analysis. All simulations were run at 193nm illumination.

3. SIMULATION DATA

The real and imaginary edge contributions were calculated for chromeless Alt-PSM and MoSi Att-PSM. Each mask was evaluated at pitch of 2, 3, and 5 wavelengths through incidence angles ranging from on-axis to 20° in air. All simulations used a 2nm cell grid with periodic boundary conditions on the sides and perfectly match layers (PML) on the top and bottom. As described above, for each combination of pitch and angle, the duty cycle was varied to locate the minimum E-field transmission. The incident wave source was located in the Quartz mask and normalized to amplitude of 1. The edge data calculated for each mask follows.

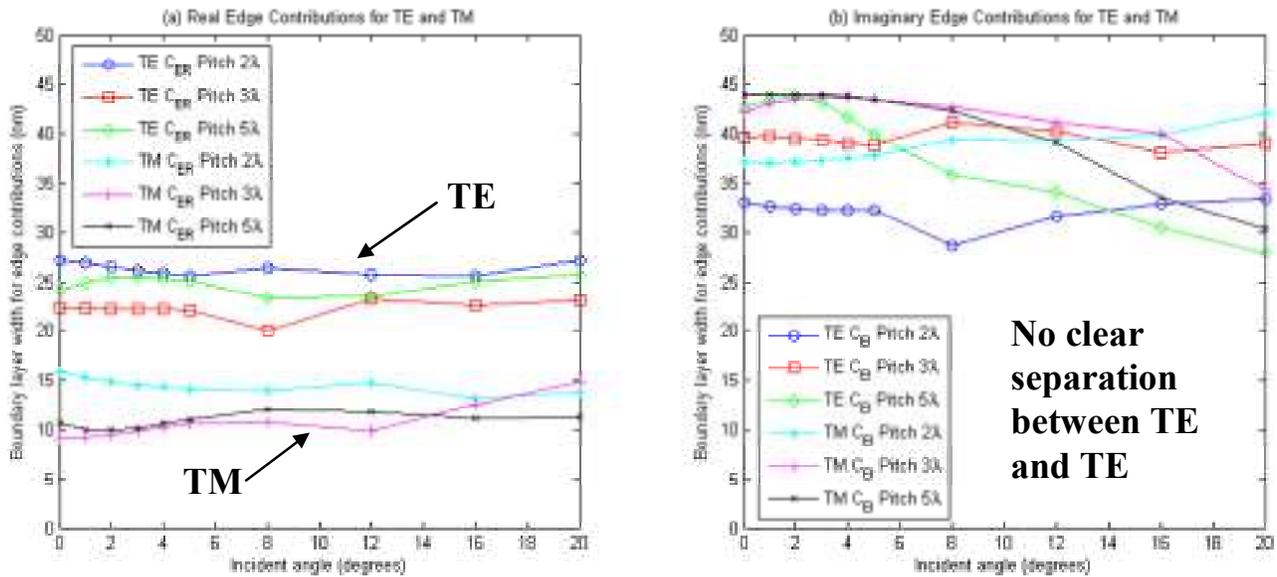### 3.1 Chromeless Alternating Phase Shift Mask

CPL technology (layout shown in Figure 3) offers the simplest geometry because the mask is made of only one material, but it is also notorious for its susceptibility to EM effects, largely due to the lossless nature. The simulations were run with a refractive index for quartz of 1.5 and a 193nm etch to produce an 180° phase shift. TMA predicts a null in the 0th order field at 50% duty cycle since the phase shifting region is lossless.

An example of the 0th order field amplitude plotted through duty cycle is shown in Figure 3 for a pitch of 2 wavelengths at several different incident angles. The dotted grey line shows where the expected TMA minimum should be. The actual value falls roughly 7% higher in terms of duty cycle. For a pitch of 386nm (2λ), 7% corresponds to a per edge effect of 14nm (0.07λ). Additionally the observed leakage at the null actually occurs between 20% and 23%. The result is an equivalent 90° boundary per edge of 38 nm to 45nm (0.23λ). The exact biases for the chromeless mask are shown in Figure 4.
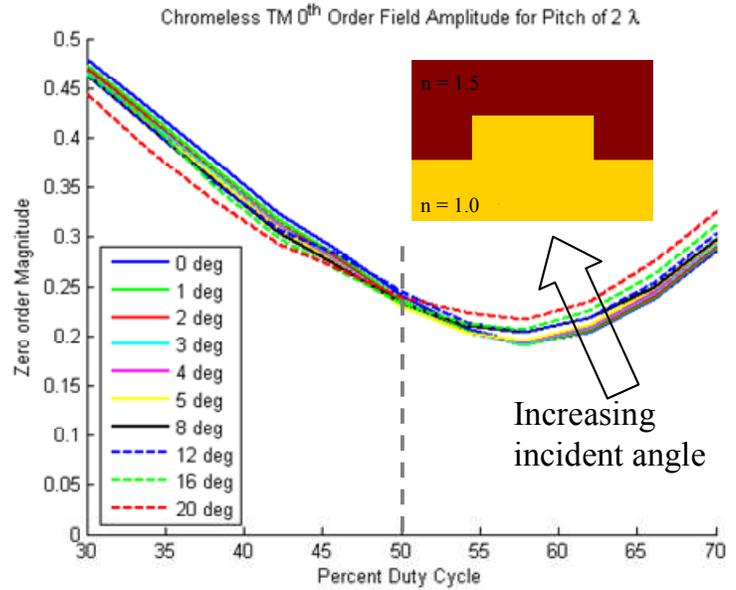
Figure 3: Fixed period 0th order transmission for CPL Alt-PSM at various incident angles

The real bias for CPL is not strongly dependent on angle; however, there is clear polarization dependence. TE (E-field parallel to the lines) requires about twice the real bias correction compared to TM (H-field parallel to the lines). Additionally, the pitch dependence is weak, showing only a 5 nm spread within polarization. The imaginary correction term is larger with C_{EI} values from 30 to 45nm per edge. This effect is significant, up to 0.2λ per edge, but there is less distinction between polarizations. The TE polarization shows more variability than the TM.

Figure 4: Chromeless mask (a) Real bias plotted vs. incident angle for several pitches (b) 90o bias plotted vs. incident angle for several pitches

3.2 MoSi Attenuating Phase Shift Mask

The same analysis was carried out for the MoSi Att-PSM (layout shown in figure 5). Here a MoSi layer of 72nm was used for the phase shifting and attenuating element. The phase shift calculated from an on-axis simulation is 175.73°, with a transmission through MoSi of 23.2% field amplitude or 5.4% intensity transmission. The phase shift was calibrated to slightly less than 180° to counteract the slightly further path difference for off-axis incidence. In practice, the phase shift can only be correct for one incident angle. By calculating the ratio of transmission between the 2 regions (100% for air, 23.2% for MoSi) the expected minimum would occur at a duty cycle where 18.9% of the pitch is air gap, with the rest covered by MoSi. Figure 5 shows a plot of the 0th order field amplitude for a pitch of 2λ.

Here the observed 10% shift in the minimum transmission duty cycle with a 386nm pitch corresponds to a real edge bias of 19nm per edge. The 5% minimum field transmission translates to a 9nm per edge imaginary bias.
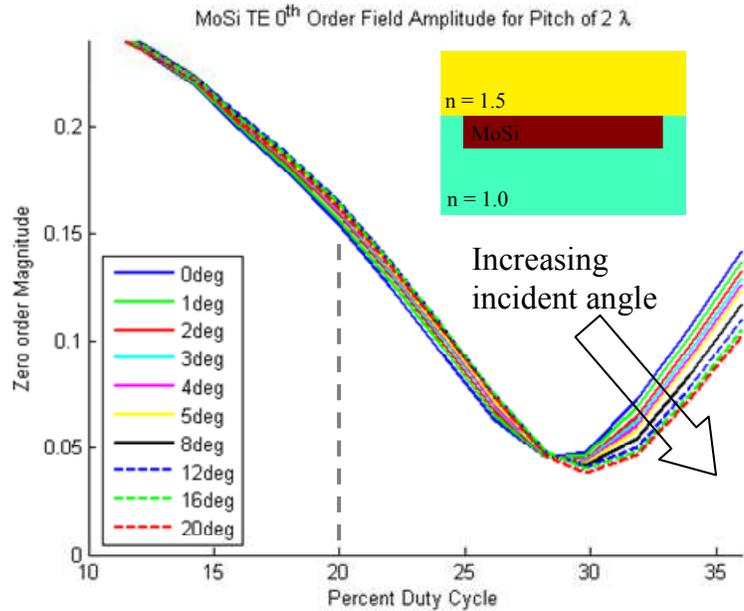

Figure 5: Fixed period 0th order transmission for MoSi Att-PSM at various incident angles

A summary of the real and imaginary biases for various incidence angles and polarization are given in Figure 6. The MoSi mask shows little change through angle for both polarizations. Also, the spread remains less than 5 nm through pitch. There is clear polarization dependence for both the real and imaginary bias terms. TM requires a smaller real bias, but a larger imaginary bias. Compared to chromeless, MoSi requires smaller corrections, especially for the quadrature component.
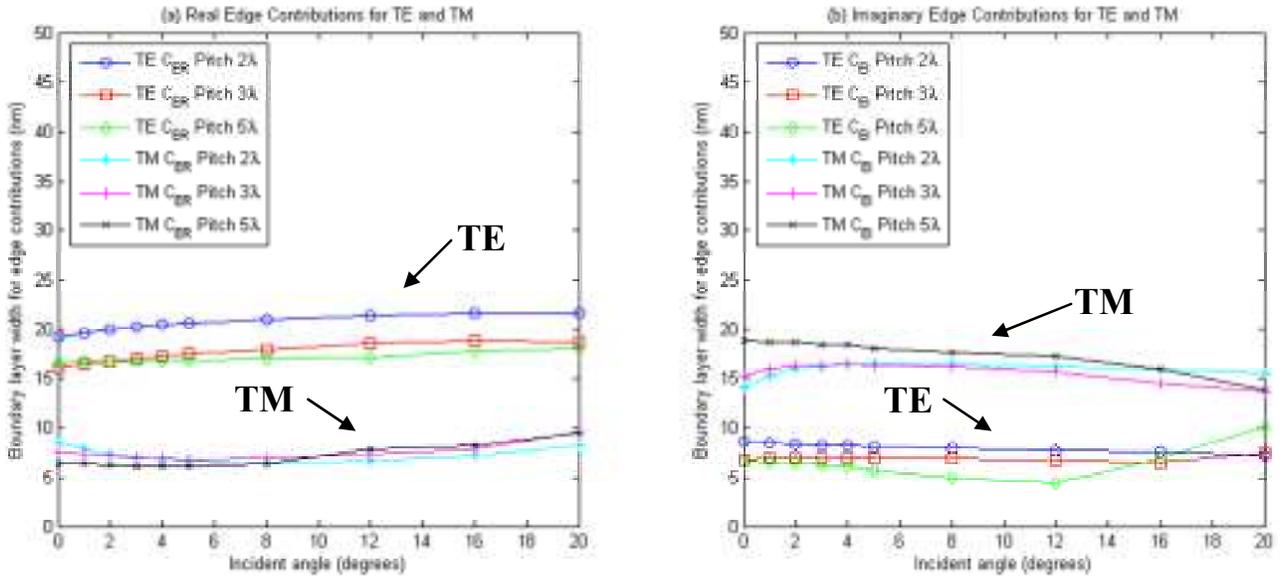
Figure 6: MoSi mask (a) CER plotted vs. incident angle for several pitches (b) CEI plotted vs. incident angle for several pitches

4. 3-D FIELD ANALYSIS
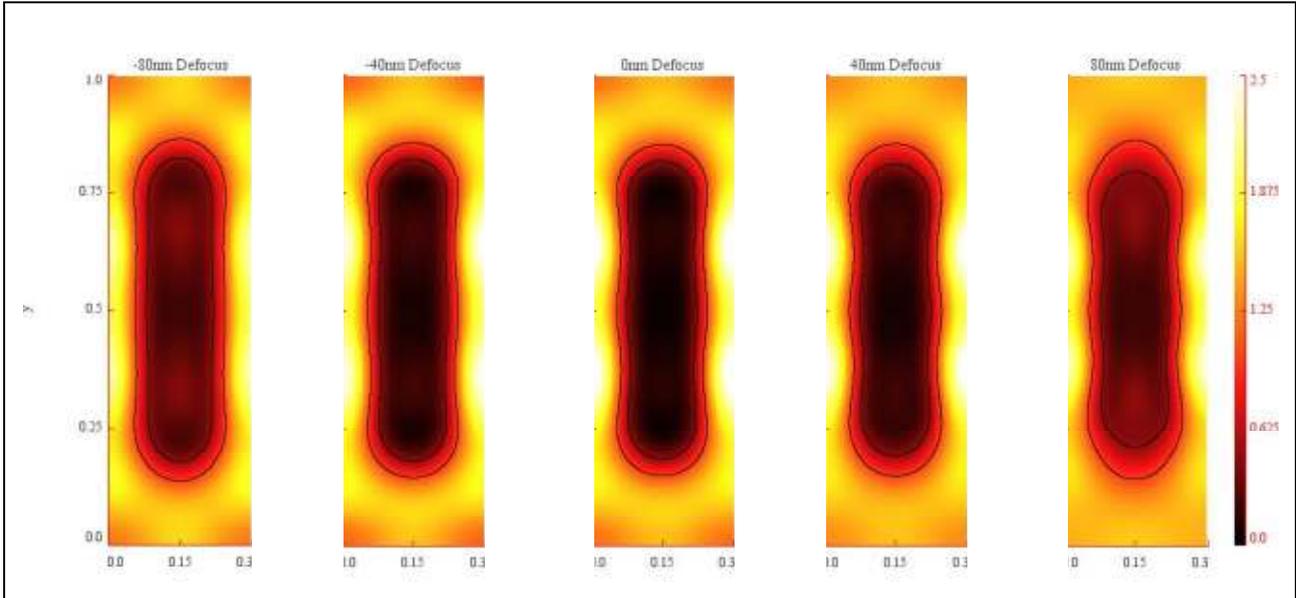
Figure 7: Contour plots generated from aerial image simulations in Panoramic using TEMPEST fields and varying amounts of defocus

In addition to the 2-D simulations described in the previous section, 3-D simulations were used to look at the effect of these biases on line ends and LES. A MoSi line 200nm x 1200nm on mask was simulated with on-axis illumination using TEMPEST. A cut line of the propagating fields was then loaded into Panoramic to compute the aerial image and observe the on wafer effects through focus. For the aerial image calculation, $\sigma = 0$ was used to emulate plane wave illumination with NA = 1.0 and 2x reduction. Figure 7 shows the aerial image produced through varying levels of
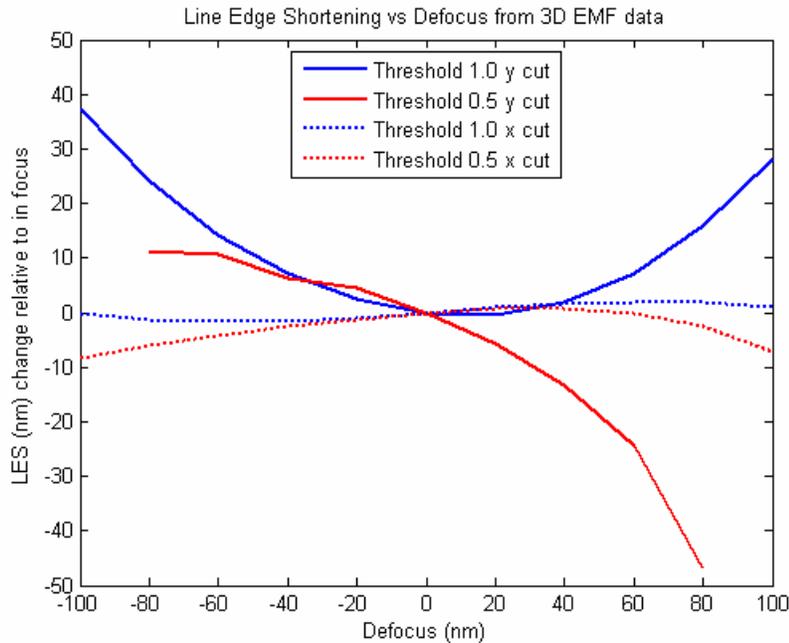
Figure 8: Plots of the Line Edge Shortening (y cut) and Line Width Shortening (x cut) through defocus

defocus. The line end regions of the images at -80 nm and +80 nm defocus clearly show asymmetry through focus. This asymmetry cannot be produced by a real (and/or 180°) mask transmission function and is an indication that the ends of the Att-PSM have significant imaginary transmission.
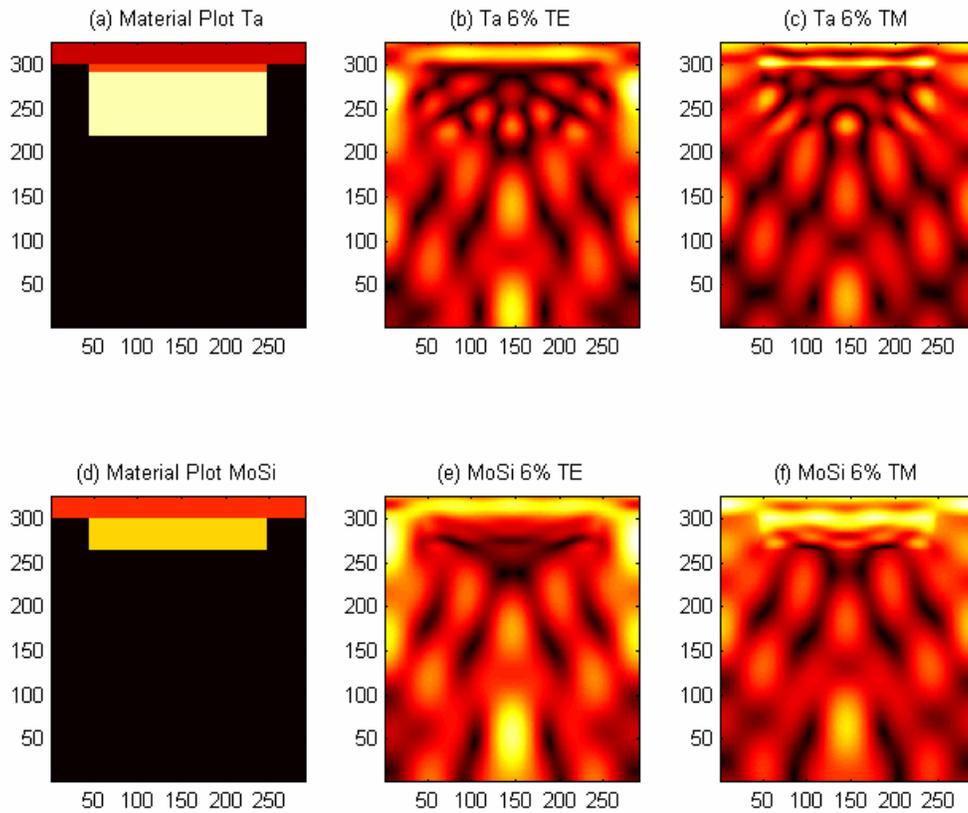
Figure 8 shows the resulting CD measurements in both the x and y directions taken at the middle of the feature. For the in focus case, the feature was 705nm by 188nm for a threshold of 1.0, and 636nm by 145nm for threshold of 0.5. The threshold values are in arbitrary units of intensity. Figure 8 shows the deviation from the in focus values. As expected, the effect is more severe for the line ends (y cuts) compared to the sides (x cuts). Also, for the 2 threshold values, the contours move in the opposite direction, larger for a threshold of 1. This implies degradation in the image contrast as well.

5.   ALTERNATE MASK STACKS

A similar analysis as described in section 3 was carried out for Ta-SiO$_2$ mask stacks of 6% and 1% transmission. The 6% mask had 18nm of Ta and 144 nm of SiO$_2$, while the 1% had 30nm thick Ta and 138nm of SiO$_2$. Even for on-axis illumination, the plots for varying duty cycle, shown below in Figure 9, do not show the clear trends present with the other mask geometries. This implies that there are additional effects complicating the transmission through the mask stack.
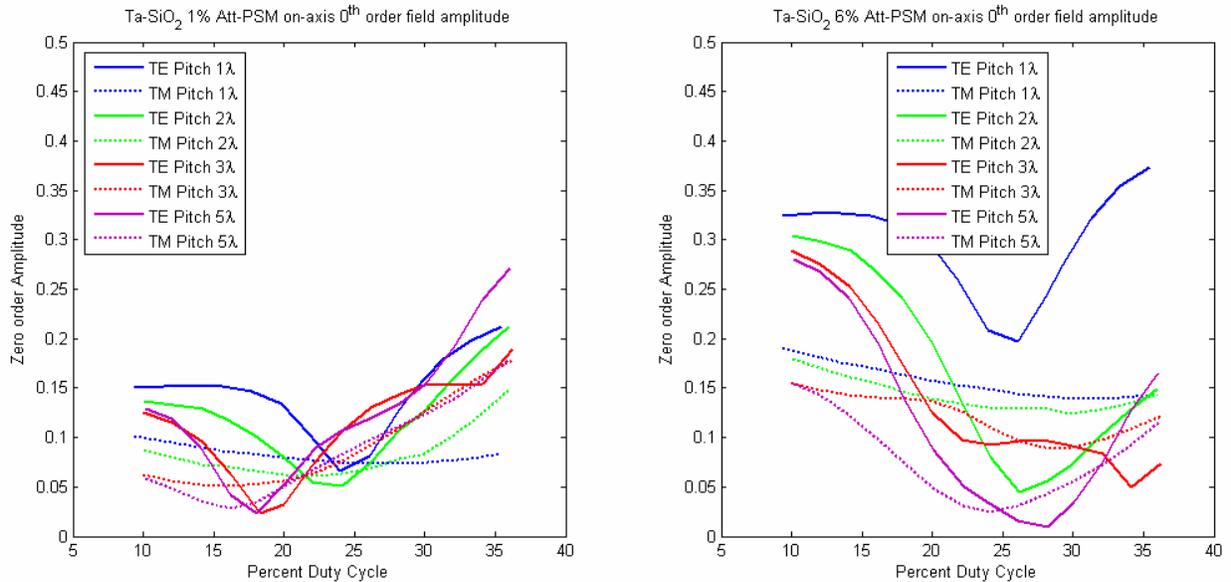
Figure 9: On-axis 0th order transmission for several pitches with the two Ta-SiO2 Att-PSM types.

(a) Material Plot Ta **(b) Ta 6% TE** **(c) Ta 6% TM**

(d) Material Plot MoSi **(e) MoSi 6% TE** **(f) MoSi 6% TM**

Figure 10: Field plots for Ta-SiO2 and MoSi masks illuminated on-axis.

There are a couple possible explanations. Unlike the other masks, Ta-SiO2 is made up of multiple layers which could produce wave guiding effects carrying energy laterally through the structure. Additionally, compared to MoSi, Ta is a better conductor, which attenuates the fields in a shorter distance. This could lead to large current sources appearing at the edges in the Ta layer and producing cross-talk across the gap. Figure 10 shows a field comparison for the Ta mask compared to MoSi for a pitch of 3l and duty cycle of 30% air gap. In the radiation zone several wavelengths away from the mask bottom, the field structure for both types of masks appear similar; however, within the mask stack, there are far more high frequency components present in the Ta mask.

6. CONCLUSIONS

Edge effects on phase shifting masks were examined through rigorous FDTD simulation. A previously presented methodology was extended to include the effects of off-axis illumination. The shift in real transmission was well behaved through incident angle variation out to 20° for both MoSi and CPL masks indicating that an angle independent TMA bias is accurate for lines and spaces. There was also clear polarization dependence, as TE polarization required twice the shift as TM. CPL required a shift (real component) of 0.1λ and 0.05λ to model the TE and TM edge sources respectively. For CPL, the equivalent boundary widths in the imaginary term in the TMA were as high as 45 nm (0.23λ). For the MoSi mask, the real and imaginary boundary widths were 0.1λ and 0.05λ for TE and TM, but 0.05λ and 0.1λ for the imaginary boundary layer.

Simulations with 3-D geometries were used to test line end effects by imaging through focus to reveal the quadrature field component. The LES asymmetry through focus was about 18 nm for 45 nm for features over a focal range of -80 nm to +80 nm. This through focus asymmetry is at least 5 times more pronounced than that for lines and spaces. Ta-SiO$_2$ showed considerable EMF effects in the mask stack. Large standing waves appeared in the oxide and edge to edge coupling through scattering from the Ta layer is the suspected culprit.

7. ACKNOWLEDGEMENTS

REFERENCES

[1] Bob Gleason and Wen-hao Cheng, "Optical properties of alternating phase-shifting masks", Proc. SPIE Vol. 6349, October 2006.

[2] Michael S. Hibbs and Timothy A. Brunner, "Phase Calibration for Attenuating Phase-Shift Masks," Proc. SPIE Vol 6152, March 2006.

[3] J. Tirapu-Azpiroz, A. E. Rosenbluth, K. Lai, C. Fonseca, and D. Yang, "Critical Impact of EMF Effects on RET and OPC Performance for 45nm and Beyond," *JVST B* 25, p. 164, 2007.

[4] C. Pierrat, A. Wong, and S. Vaidya, "Phase-shifting mask topography effects on lithographic image quality", Electron Devices Meeting, Dec 1992.

[5] J. Tirapu-Azpiroz and E. Yablonovitch, "Incorporating mask topography edge diffraction in photolithography simulations," J. Opt. Soc. Am. A **23**, 821-828 (2006)

[6] Shoji Hotta, Thomas V. Pistor, Konstantinos Adam, Andrew R. Neureuther, "Effects of shifter edge topography on through focus performance," Proc. SPIE Vol. 4186, p. 827-837, Jan 2001.

[7] Konstantinos Adam and A. R. Neureuther, "Simplified models for edge transitions in rigorous mask modeling," Proc. SPIE Vol. 4346, p. 331-344, Sept 2001.

[8] A. K. Wong and A. R. Neureuther, "Mask topography effects in projection printing of phase-shifting masks," IEEE Trans. Electron Devices 41, 895–902 (1994).

[9] David J. Gerold, Josh S. Petersen, and Marc D. Levenson, "Multiple Pitch Transmission and Phase Analysis of Six Types of Strong Phase-Shifting Masks," Proc. SPIE Vol. 4346, September 2001, pp. 729-743.

[10] James V. Beach, John S. Petersen, et. al., "Evaluation of SCAA Mask Technology as a Pathway to the 65nm Node," Proc. SPIE Vol. 5040, June 2003, pp. 1103-1114.

[11] Marshal A. Miller, A. R. Neureuther, Daniel P. Ceperley, Juliet Rubinstein, and Koji Kikuchi, "Characterization and Monitoring of Edge Effects in Photomasks," Proc. SPIE Vol. 6730, October 2007.

[12] Ibid 11